

Pupil-segmentation-based adaptive optical correction of a high-numerical-aperture gradient refractive index lens for two-photon fluorescence endoscopy

Chen Wang^{1,2} and Na Ji^{2,*}

¹State Key Laboratory of High Field Laser Physics, Shanghai Institute of Optics and Fine Mechanics, Chinese Academy of Sciences, P.O. Box 800-211, Shanghai 201800, China

²Janelia Farm Research Campus, Howard Hughes Medical Institute, 19700 Helix Drive, Ashburn, Virginia 20147, USA

*Corresponding author: jin@janelia.hhmi.org

Received March 9, 2012; accepted April 10, 2012;
posted April 13, 2012 (Doc. ID 164448); published May 30, 2012

The intrinsic aberrations of high-NA gradient refractive index (GRIN) lenses limit their image quality as well as field of view. Here we used a pupil-segmentation-based adaptive optical approach to correct the inherent aberrations in a two-photon fluorescence endoscope utilizing a 0.8 NA GRIN lens. By correcting the field-dependent aberrations, we recovered diffraction-limited performance across a large imaging field. The consequent improvements in imaging signal and resolution allowed us to detect fine structures that were otherwise invisible inside mouse brain slices. © 2012 Optical Society of America

OCIS codes: 110.1080, 110.0180.

A gradient-index (GRIN) cylinder with a refractive index maximum at the cylinder axis and a radial refractive-index profile of parabolic shape has the same imaging and transforming rules as those for homogeneous lenses [1]. Because of their small sizes, light weight, and relatively low cost, these GRIN lenses have become an attractive alternative to conventional lenses for many applications from optical communication [2] to endoscopy [3]. Similar to homogeneous lenses, GRIN lenses also suffer from on-axis and off-axis aberrations, which limit the effective imaging field of view (FOV) and degrade imaging quality. Recently, aberration corrections of GRIN lenses with adaptive optics (AO) have been demonstrated both for confocal microscopy [4] and multi-photon fluorescence microscopy [5]. In those studies, the GRIN lenses were of relatively low NA (≤ 0.5), the aberrations were corrected by low-order deformable mirrors, and only on-axis aberrations were considered. In this letter, we used the pupil-segmentation-based AO approach, which we recently developed and implemented both *in vitro* [6] and *in vivo* [7], to correct the intrinsic aberrations of a high-resolution compound GRIN lens with 0.8 NA. We focused on this particular lens because, when working at its diffraction-limited resolution, it can resolve subcellular structures and thus, have great potential for a wide variety of bioimaging applications [8]. It also suffers from large off-axis aberrations and has an effective FOV of a diameter of tens of micrometers [9]. Using our AO method, we measured optical aberrations at different field positions, which allowed us to recover diffraction-limited performance over a large FOV and improve signal intensity up to ~ 14.5 fold for field positions $100 \mu\text{m}$ away from the center.

We built an AO two-photon endoscopy system by incorporating a commercial GRIN lens (GRINTECH GmbH, GT-MO-080-0415-810, $1.92\times$, object NA = 0.8, image NA = 0.415) designed for high-NA two-photon imaging into a home-built AO scanning two-photon fluorescence microscope described previously [6,7]. The top surface of GRIN lens was placed $100 \mu\text{m}$ below the focal

plane of an air objective in accordance with the GRIN lens' image working distance. The air objective (Nikon, CFI Plan Apochromat Lambda, $10\times$, NA = 0.45) was slightly underfilled to match the image NA of the GRIN lens. The position of the GRIN lens was precisely adjusted to ensure a symmetric beam intensity distribution after the beam exited the GRIN lens. The distance between the GRIN lens and the sample is controlled by a long-travel piezo stage (Physik Instrumente, M-501). A Ti:sapphire femtosecond oscillator (Coherent, Inc., Chameleon Ultra II) tuned to 900 nm provided the two-photon fluorescence excitation.

We used an image-based AO approach to measure and correct the optical aberrations. Briefly, we illuminated only one segment of the objective back pupil and obtained an image in the usual manner by scanning. If the light ray from this pupil segment was deflected by aberrations along its path, the fluorescence image formed would be shifted from the image obtained under full-pupil illumination. From the magnitude and direction of this shift, the local wavefront tilt could be calculated. After the whole pupil was sampled in this fashion, a corrective wavefront could then be reconstructed from the local wavefront tilts, just as in a Shack-Hartmann wavefront sensor [6]. In this experiment, we measured the wavefront tilts at 81 distinct pupil positions by illuminating pupil segments with $1/25$ of the full pupil area and measuring the image shifts of $2 \mu\text{m}$ diameter fluorescent beads on coverglass. We used a liquid crystal spatial light modulator (SLM) (Boulder Nonlinear Systems, 512×512 active-pixel PhaseFlat phase-only nematic liquid crystal SLM) conjugated to the back pupil of the Nikon objective for aberration compensation. The SLM area used for AO correction was inscribed to the circular back pupil of the endoscope. With hundreds of thousands of active pixels, the SLM provided us superior wavefront control [6,7].

First, we measured the aberration of our imaging setup without the GRIN lens and found its root mean square (RMS) deviation to be $0.047 \mu\text{m}$ or $\lambda/19$. We then characterized the on-axis aberrations of the GRIN lens with

fluorescent beads located at the center of the FOV. Because this GRIN lens has a highly curved focal surface, for a large FOV, we imaged the sample at $0.5\ \mu\text{m}$ axial steps and presented their maximal intensity projections (Fig. 1). AO correction increased the signal intensity in the central FOV [Figs. 1(a) and 1(d)]. The corrective wavefront [Fig. 1(c)] showed characteristics that were invariant from day to day, but did rotate with the different mounting azimuthal orientations of the GRIN lens, suggesting that the observed aberrations were indeed intrinsic to the GRIN lens itself. Using the same corrective pattern, we also imaged fixed brain slices of a YFP line 16 transgenic mouse and observed image quality improvements on both the somata and the much finer neuropils, with many more fine processes resolvable after AO correction [Figs. 1(b) and 1(e)]. The peak signal of the $2\ \mu\text{m}$ diameter beads at the central FOV increased by 80% after AO correction. However, no visible image quality enhancement was detected at the edge of the FOV [Fig. 1(d)], because the off-axis aberrations were not accounted for by the on-axis correction.

To characterize the off-axis aberrations of the GRIN lens, we measured the aberrations at eight off-axis locations $100\ \mu\text{m}$ away from the field center: $(0, -100)$, $(0, 100)$, $(-100, 0)$, $(100, 0)$, $(-70.7, -70.7)$, $(70.7, 70.7)$, $(-70.7, 70.7)$, $(70.7, -70.7)\ \mu\text{m}$, in addition to the aberrations at field center $(0, 0)$ (Fig. 2). The focal series images for beads at these off-axis locations [e.g., Figs. 2(a) and 2(b) for field positions $(-70.7, -70.7)$ and $(0, -100)\ \mu\text{m}$] indicated severely degraded imaging quality, in agreement with the large wavefront aberrations measured at these positions [e.g., Figs. 2(c) and 2(d)]. We compared the integrated signal of the bead images at different focal planes before and after AO correction for all nine field positions [Fig. 2(e)]. For the central FOV [green curve, Fig. 2(e)], the improvement was moderate, similar to those in Fig. 1. For the off-axis locations [red curves, Fig. 2(e)], the improvements were drastic. For all field

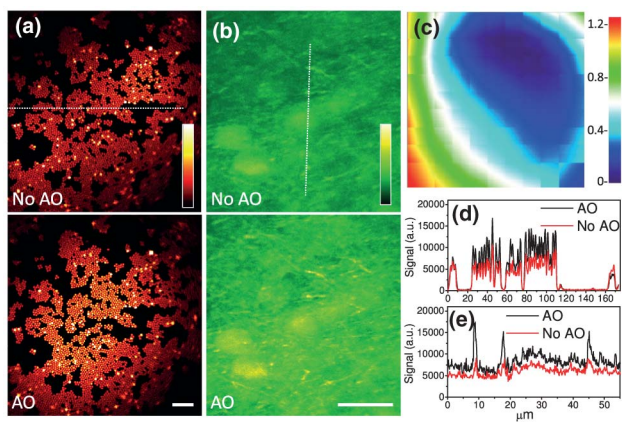


Fig. 1. (Color online) On-axis AO correction of a 0.8 NA endoscope. (a) Maximal intensity projections of $2\ \mu\text{m}$ diameter fluorescent beads on coverglass before and after AO correction at the center of the FOV. (b) Maximal intensity projections of a brain slice of a YFP line 16 mouse without and with the AO correction in (a). (c) Aberration correction pattern in units of wavelength ($\lambda = 900\ \text{nm}$). (d), (e) Signal profile along the two dashed lines in (a) and (b), respectively. Scale bars: $20\ \mu\text{m}$.

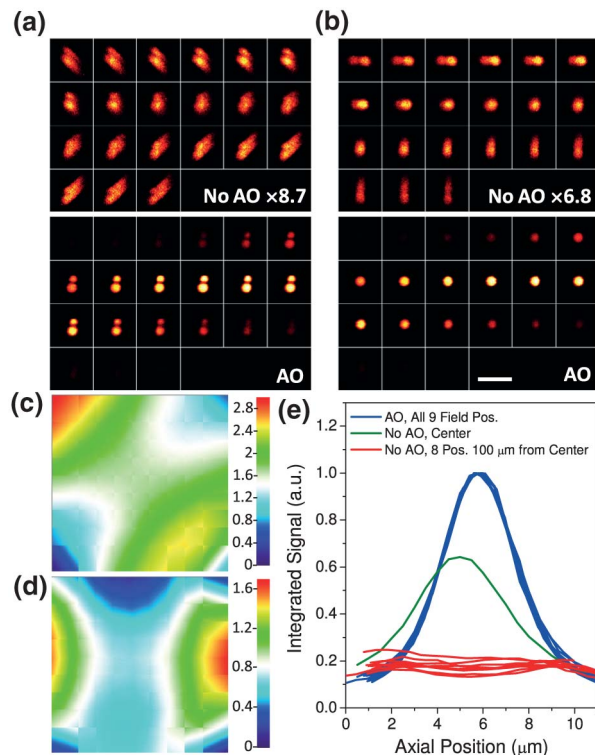


Fig. 2. (Color online) Off-axis AO correction of a 0.8 NA endoscope. (a) Focal series images of two fluorescent beads located at $(-70.7, -70.7)\ \mu\text{m}$ field position before and after AO correction; Images without AO have its brightness digitally enhanced by $8.7\times$ so that both focal series have the same maximal signal. Focal step is $0.5\ \mu\text{m}$. (b) Similar images to those in (a) obtained at $(0, -100)\ \mu\text{m}$. Digital enhancement for images without AO is $6.8\times$. (c) and (d) are the aberration correction patterns for (a) and (b), respectively, in units of wavelength. (e) Integrated signal of focal series images at different focal planes for 9 field positions: $(0, 0)$, $(0, -100)$, $(0, 100)$, $(-100, 0)$, $(100, 0)$, $(-70.7, -70.7)$, $(70.7, 70.7)$, $(-70.7, 70.7)$, $(70.7, -70.7)\ \mu\text{m}$. For each field position, the integrated signal measured without AO is normalized to that measured with AO. Scale bars: $10\ \mu\text{m}$.

positions, after AO correction, diffraction-limited resolution was recovered, with similar FWHMs for the axial profiles of the integrated signal [$3.7 \pm 0.1\ \mu\text{m}$ for the nine blue curves in Fig. 2(e)]. Besides the improvement in imaging resolution, the signal was also greatly enhanced. Focal series without AO correction have their maximal signal occur at axial planes where lateral resolution was obviously degraded [e.g., the 6th frame in the upper panel of Fig. 2(a)]. AO correction increased this maximal signal by $8.7\times$ and $6.8\times$, respectively. When the maximal signal at the medial focal plane [“circle of least confusion,” e.g., the ninth frame in the upper panel of Fig. 2(a)] was used for comparison, the signal improved by $14.5\times$ and $10.4\times$, respectively [Figs. 1(a) and 1(b)].

Using the correction patterns obtained above, we imaged samples with large FOV. For a $200\ \mu\text{m} \times 200\ \mu\text{m}$ field of beads, using the AO corrections at all nine field positions, we improved the image across the entire area, thus, effectively extended the applicable imaging FOV [Figs. 3(a) and 3(b)]. The improvement was particularly striking at the edges and corners of the FOV, where the

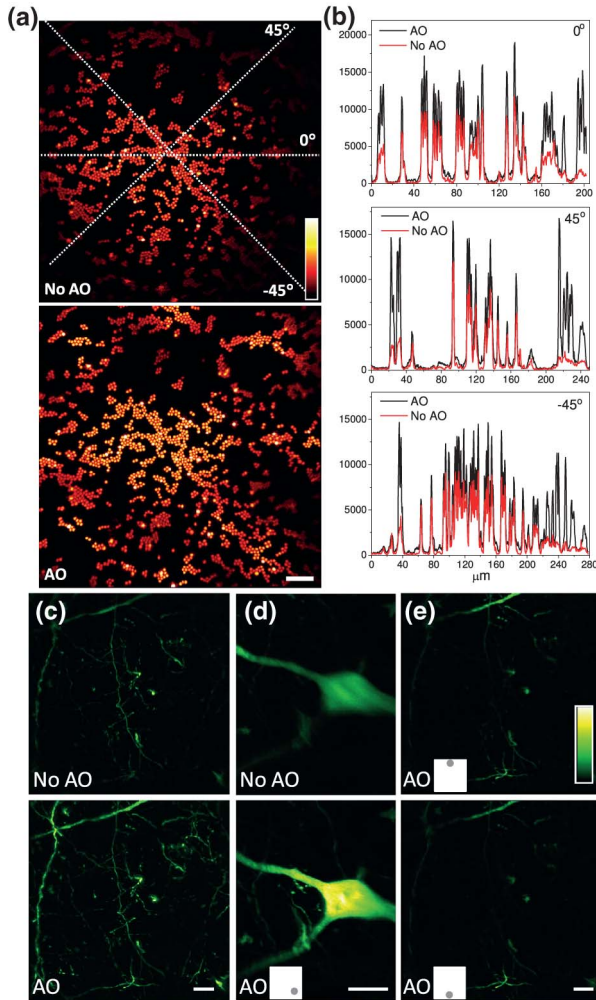


Fig. 3. (Color online) Enlarged FOV of a 0.8 NA GRIN lens endoscope with AO correction. (a) Maximal intensity projections of $2\ \mu\text{m}$ diameter beads in a $200\ \mu\text{m}$ image field without and with AO corrections; Image with AO correction is the maximal intensity projection of images taken with nine AO correction patterns. (b) Signal profiles along the three dashed lines in (a). (c) Maximal intensity projections of a brain slice before and after AO corrections at nine field positions. (d) Maximal intensity projections of another brain slices at $(70.7, -70.7)\ \mu\text{m}$ before and after AO correction there. (e) Maximal intensity projections of the brain slice in (c) after AO corrections at opposing field positions $(0, 100)$ and $(0, -100)\ \mu\text{m}$. Insets describe the image field positions where AO correction was carried out. Scale bar: $20\ \mu\text{m}$.

off-axis aberration corrections were done. This enlargement of imaging FOV would prove especially useful in bioimaging applications where it is impractical to move the GRIN lens relative to the sample in the lateral directions. As a proof of principle, we imaged a fixed brain slice of a GFP line M mouse using the same field-dependent aberration corrections. Similar to the observations on

fluorescent beads, we could now image the structures located away from the center of the FOV after AO corrections [Fig. 3(c)]. Also, similar to the bead samples, at off-axis locations, the improvements in both signal and resolution were striking, with subcellular structures that were invisible before AO correction now clearly resolvable [Fig. 3(d)].

Interestingly, we found that the correction pattern at one off-axis location would improve the signal at the opposing field position. For example, correction at the top of the FOV improved image quality at the bottom of the field, and vice versa [Fig. 3(e)], which suggests that the two opposing field positions share some of the same aberration components. Ray-tracing with ZEMAX on a GRIN objective lens (GRINTECH GmbH, GT-IFRL-200-inf-50-570-Gradient5) confirmed that field positions that are centrally symmetric with respect to the field center always have similar astigmatism, the major aberration component at large field angles. Therefore, when the aberration correction is applied for one corner, it also corrects the astigmatism at the opposite end, and consequently, improves the image quality there. More generally, the circular symmetry of ideal GRIN lenses may allow corrections measured at differing off-axis distances to be used at many field positions after proper rotational transformations; thus, significantly reducing the number of AO corrections needed to cover a large FOV.

In conclusion, we have successfully demonstrated the use of pupil-segmentation-based AO to correct the inherent aberrations of GRIN lens with a high NA. We measured and corrected the aberration at different field positions and achieved diffraction-limited performance for an extended FOV. For those applications where high resolution and large FOV are needed, AO would prove to be an essential component of a modern endoscope.

The research is supported by the Howard Hughes Medical Institute. We thank Dr. Aaron Kerlin for an inspiring discussion.

References

1. C. Gomez-Reino, M. V. Perez, and C. Bao, *Gradient-Index Optics* (Springer-Verlag, 2002).
2. W. J. Tomlinson, *Appl. Opt.* **19**, 1127 (1980).
3. J. C. Jung and M. J. Schnitzer, *Opt. Lett.* **28**, 902 (2003).
4. W. M. Lee and S. H. Yun, *Opt. Lett.* **36**, 4608 (2011).
5. F. Bortoletto, C. Bonoli, P. Panizzolo, C. D. Ciubotaru, and F. Mammano, *PLoS ONE* **6**, e22321 (2011).
6. N. Ji, D. E. Milkie, and E. Betzig, *Nat. Meth.* **7**, 141 (2010).
7. N. Ji, T. R. Sato, and E. Betzig, *Proc. Nat. Acad. Sci. USA* **109**, 22 (2012).
8. R. P. Barretto, B. Messerschmidt, and M. J. Schnitzer, *Nat. Meth.* **6**, 511 (2009).
9. GRINTECH. Datasheet "High NA for 2-Photon Microscopy," available from <http://www.grintech.de/grin-lens-systems-for-medical-applications.html>.